

Range aliasing in frequency coherent geoacoustic inversion

Caglar Yardim, Peter Gerstoft, and William S. Hodgkiss

Marine Physical Laboratory, Scripps Institution of Oceanography, La Jolla, California 92093-0238
cyardim@ucsd.edu, gerstoft@ucsd.edu, whodgkiss@ucsd.edu

Abstract: This paper discusses the effects of frequency selection on source localization and geoacoustic inversion methods that use frequency coherent objective functions. Matched-field processors based on frequency-coherent objective functions often have rapidly fluctuating range ambiguity surfaces. Insufficient sampling in frequency domain results in range aliasing terms that affect geoacoustic inversion. Range aliasing and its effects on source localization and environmental parameter inversion are demonstrated on data collected during the MAPEX2000 experiment. Guidance for frequency selection to avoid range aliasing is provided.

© 2011 Acoustical Society of America

PACS numbers: 43.60.Ac, 43.60.Jn, 43.30.Pc [JC]

Date Received: June 21, 2011 Date Accepted: August 6, 2011

1. Introduction

An important characteristic of frequency-coherent processors is the rapid fluctuations in source range ambiguity.¹⁻³ These are caused in part by the environment due to complicated waveguide effects. However, most range-oscillations are caused by the repetitive appearance of the main lobe at erroneous ranges as aliased lobes. It is shown that this is caused by frequency undersampling and the effects usually are larger than those caused by the environment. When these repetitive aliased lobes get dense, they overshadow the environmental effects. This affects significantly the source localization and can be projected into the geoacoustic parameter space as uncertainty and/or a bias. Range aliasing previously has been encountered in frequency coherent geoacoustic inversion (e.g., Fig. 8 in Ref. 1 and Fig. 1 in Ref. 2). Reference 3 provides a nice description of the phenomena without analysis. Here we provide a mathematical framework and an approach to proper frequency selection in order to avoid aliasing.

Typically geoacoustic inversion uses some form of Bartlett power $B(\mathbf{m})$ for an environment represented by a vector of geoacoustic and source parameters \mathbf{m} . The conventional Bartlett processor (array coherent, frequency incoherent) $B_a(\mathbf{m}, f_i)$ is computed coherently across the array for each frequency and averaged incoherently across frequency to obtain⁴

$$B_a(\mathbf{m}) = \frac{1}{NN_f} \sum_{j=1}^N \sum_{i=1}^{N_f} |\mathbf{w}_a^H(\mathbf{m}, f_i) \mathbf{y}_a^j(f_i)|^2, \quad (1)$$

where $\mathbf{y}_a^j(f_i)$ and $\mathbf{w}_a(\mathbf{m}, f_i)$ are j th snapshot of the measured data and the normalized replica vectors across the array at frequency f_i , respectively. N and N_f are the numbers of data snapshots and frequencies used.

The frequency-only coherent objective function⁵ is computed coherently across frequency and averaged incoherently across the array elements. Assuming data $\mathbf{y}_f(a_i)$ and replica field vectors $\mathbf{w}_f(\mathbf{m}, a_i)$ across the frequencies for array element a_i

$$B_f(\mathbf{m}) = \frac{1}{NN_a} \sum_{j=1}^N \sum_{i=1}^{N_a} |\mathbf{w}_f^H(\mathbf{m}, a_i) \mathbf{y}_f^j(a_i)|^2, \quad (2)$$

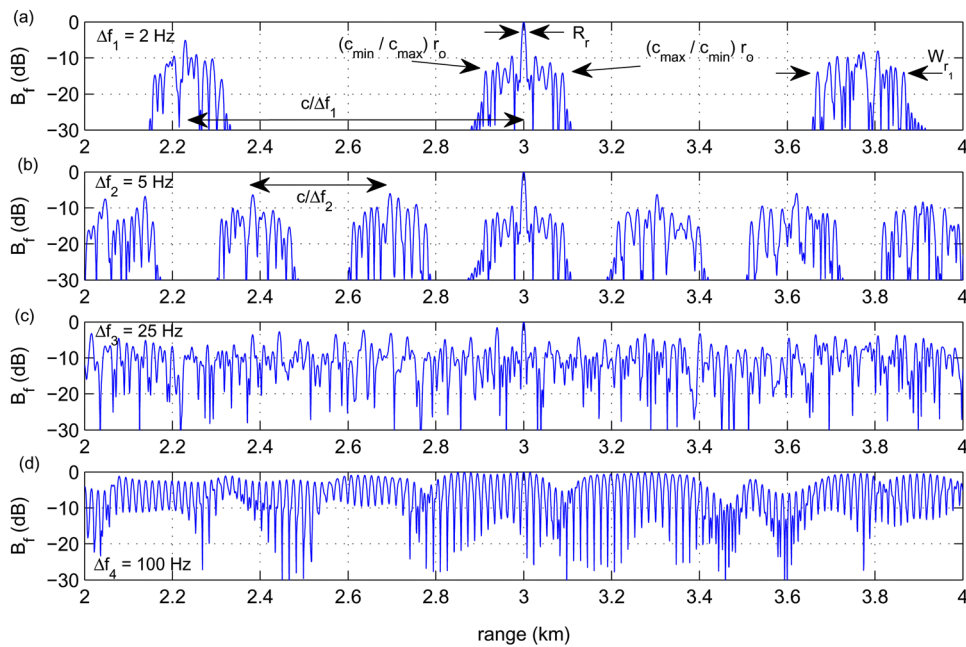


Fig. 1. (Color online) $B_f(r)$ for $\Delta f = 2, 5, 25,$ and 100 Hz on a waveguide supporting $N_m = 5$ modes with $c(n) = 1510, 1515, 1538, 1541,$ and 1553 m/s, $BW = 200$ Hz ($f = 200\text{--}400$ Hz), and $r_0 = 3$ km.

where N_a is the number of elements in the array. Note that broadband geoacoustic inversion using a single hydrophone can be performed with this method [i.e., $N_a = 1$ in Eq. (2)].^{6,7}

It also is possible to use frequency information coherently in addition to the array coherence.⁸ This fully coherent approach is computed by $B_{af}(\mathbf{m}) = 1/N \sum_{i=1}^N |\mathbf{w}^H(\mathbf{m})\mathbf{y}|^2$ with supervectors $\mathbf{w}(\mathbf{m})$ and \mathbf{y} obtained by stacking the replica vectors and data for all frequencies and array elements. Various coherent processors have been used successfully to perform geoacoustic and/or source inversion.^{1-3,8,9}

2. Range aliasing

Broadband processors enable the incorporation of information about geoacoustic parameters from multiple frequencies (coherently or incoherently), many of which have frequency dependent sensitivities. This results in robust inversions relative to narrowband processors. A common characteristic of broadband processors using frequency coherence is the oscillatory behavior in source range estimates^{2,3} caused by undersampling of the acoustic field in the frequency domain. This is similar to the temporal aliasing encountered with the inverse Fourier transform of a signal whose Fourier transform has been undersampled. Broadband geoacoustic inversion is performed for a selected set of frequencies. If there are not enough frequencies, this creates false peaks at repetitive ranges referred to as range aliases. If this undersampling is severe, the aliases will appear close to the true values, creating objective functions with multiple peaks and hence errors in the inversion especially for low SNR cases. Some examples where aliasing can occur in geoacoustic inversion include using a source that only emits a few frequencies, using a source of opportunity, or using a minimal number of frequencies since the computational cost is often proportional to the number of frequencies.

When geoacoustic inversion is done using a few frequencies, the frequency coherent Bartlett objective functions produce a main lobe around the true source range of r_0 . The main lobe consists of two parts, a high resolution peak at the true source

location surrounded by numerous side lobes. When this peak is distinct, *i.e.* the side lobes and peak do not overlap and are smaller in magnitude, frequency-coherent objective functions have significantly higher range resolutions compared to conventional Bartlett processors. For an erroneous source range estimate r^* , the phase shift across the array is almost identical in the conventional array coherent Bartlett processor. In contrast, a frequency coherent objective function results in the summation of a varying phase shift across frequencies $\mathbf{w}_f^H \mathbf{y}_f = \sum_{j=1}^{N_f} \exp(-i w_j [r - r^*] / c)$, which cancel each other quickly as $r - r^*$ increases. Therefore, the frequency coherent objective function is more sensitive to source range than the conventional Bartlett objective function.

These effects are sharper and easy to notice with well-defined side lobe structure of similar amplitudes in a simplified, non-dispersive Pekeris waveguide where mode amplitudes are assumed identical (Fig. 1). For this case, the frequency-only coherent Bartlett power can be approximated by a sinc function in the vicinity of r_0 . This results in

$$B_f(r) \approx \text{sinc}^2\left(\frac{BW}{c}(r - r_0)\right) \quad \text{and} \quad R_r \approx \frac{2c}{BW}, \quad (3)$$

where range resolution R_r is defined as $2 \times$ peak-to-first null distance, BW is the frequency bandwidth, and c is approximately the average phase speed of the propagating modes with non-negligible amplitudes.

The side lobes within this main lobe correspond to phase alignment of modes at different ranges. The Bartlett power sharply drops to zero beyond a certain distance from r_0 and the side lobes in the main lobe farthest from r_0 are determined by the phase alignment of the Bartlett function for fastest (c_{\max}) and slowest (c_{\min}) phase speeds supported by the propagating modes. Therefore, the closest and farthest side lobes ranges within the main lobe that spans W_{r_0} are

$$r_{\min_0} = \left(\frac{c_{\min}}{c_{\max}}\right)r_0, \quad r_{\max_0} = \left(\frac{c_{\max}}{c_{\min}}\right)r_0 \rightarrow W_{r_0} = \left(\frac{c_{\max}^2 - c_{\min}^2}{c_{\max}c_{\min}}\right)r_0. \quad (4)$$

In addition to the main lobe, $B_f(\mathbf{m})$ also includes aliased lobes on each side of the main lobe due to phase alignment of different frequency terms at aliased ranges. Therefore, these aliased lobes are byproducts of the Bartlett processor and frequency undersampling, and are independent of the ocean waveguide environment. The locations of these lobes for a given frequency sampling interval Δf are given by

$$r_i = r_0 + i \frac{c}{\Delta f}. \quad i = \{\dots, -1, 0, 1, \dots\}. \quad (5)$$

The width of each aliased lobe W_{r_i} can be approximated by Eq. (4), replacing r_0 with the corresponding r_i . These aliased lobes usually resemble the main lobe: A similar peak and separate side lobe structure. Even though they are aliased into other ranges, they are not exact copies of the main lobe due to the different phase speed for each mode. This can easily be seen from Eq. (5), where the alias range shift $c(n)/\Delta f$ is slightly different for each mode $n = 1 \dots N_m$. Moreover, since the true ocean waveguide is dispersive, the phase speed of the modes are a function of frequency and can vary significantly especially if the broadband source spectrum is close to the cut-off frequency of the mode. This further distorts the shapes of the aliased lobes. A feature of these aliased lobes is the range dependence of lobe width W_{r_i} since it is proportional to r_i . The lobes further in range will have larger lobe widths.

All the parameters defined above are shown in Fig. 1(a). In Figs. 1(c)–1(d), $W_{r_i} > c/\Delta f$ and the main and aliased lobes are overlapping. Note how the environmental effects (smaller side lobes) are suppressed by aliased lobe peaks as Δf increases. The entire function is dominated by aliases in Fig. 1(d), a frequently encountered case in geoacoustic inversion (e.g., Fig. 8 in Ref. 2 and Fig. 1 in Ref. 3).

3. MAPEX2000 data analysis

The effects of range aliasing are demonstrated on a HLA here, but any array could be used. The data was collected during the MAPEX2000 experiment conducted by the NURC on November 28, 2000 in a shallow water area north of Elba Island, off the Italian west coast.¹⁰ This area is characterized by a flat bottom covered with a thin clay and sand-clay sedimentary layer. The water depth is 115–120 m. The experimental setup involves a fixed source broadcasting a linear frequency modulated pulse and a 254 m long towed HLA 55–65 m deep. A frequency bandwidth of 250–500 Hz is used. The SSP in the water column exhibits a slightly positive gradient for most of the water column, except near the bottom, where there is a sharp decrease in sound speed.

Source range-depth ambiguity surfaces for $\Delta f = 100$ and 5 Hz are given in Fig. 2 by conventional (array-only), frequency-only, and fully coherent Bartlett processors for the data snapshot at $r_s = 4.1$ km and $z_s = 50$ m. The ambiguity surfaces for both Δf are somewhat flat with large side lobes in the case of B_a since HLAs have poor source localization properties¹¹ [Fig. 2(a)]. However, the conventional Bartlett processor is immune to range aliasing.

The effects of range aliasing is evident in the results of both frequency-only and fully coherent MFPs given in Figs. 2(b)–2(c). The only difference between them is the lower sidelobe levels of fully coherent case. For $\Delta f = 100$ Hz, the aliased and main lobes are on top of each other creating the highly spiky ambiguity surfaces. On the contrary, for $\Delta f = 5$ Hz, the main and aliased lobes are clearly separated with sidelobes of each lobe visible around the local peaks. Frequency coherence creates high resolution in range not depth, depicted by vertical stripes in the ambiguity surfaces with $\Delta f = 5$ Hz.

Even though insufficient frequency sampling creates significant errors in source localization, its effects on geoacoustic inversion are more subtle. It results often in biased estimates in parameters such as water depth and sediment thickness as well as

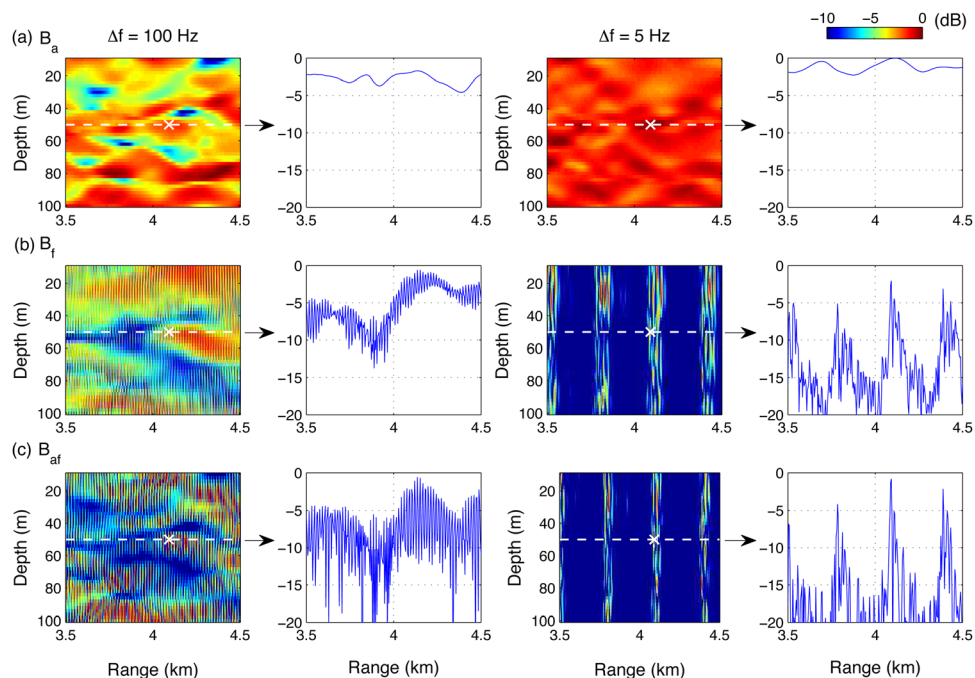


Fig. 2. (Color online) Results for MAPEX2000 data. Source range-depth ambiguity surfaces and range ambiguity plots at the true source depth (\times) for $\Delta f = 100$ and 5 Hz. (a) Array-only coherent, (b) frequency-only coherent, and (c) fully coherent processors.

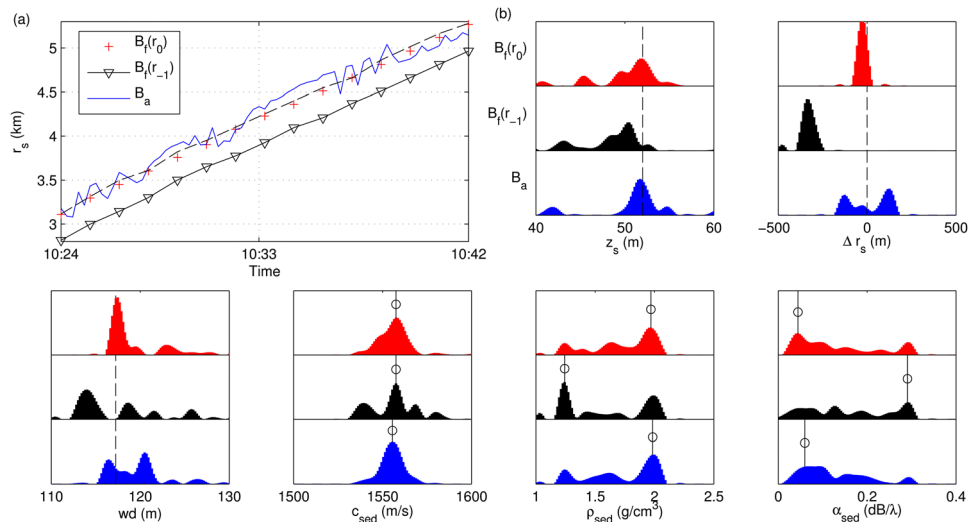


Fig. 3. (Color online) Results for MAPEX2000 data. (a) GPS measured (dashed) and inverted ranges vs time. (b) Histograms of source and geoacoustic parameter inversion results: B_f (top), B_f tracking the first alias (middle), and B_a (bottom). Vertical lines represent the true values (dashed) if measured, or MAP solutions (o) otherwise.

increased uncertainty in other sub-bottom properties. These geoacoustic parameter errors are caused by the projection of source localization error into the geoacoustic parameter space.

This is shown on the MAPEX2000 data from 10:24–10:42 UTC where the HLA moves between 3.1–5.2 km [Fig. 3]. This region is selected since the geoacoustic properties are very stable with 117 m water depth and 51.5 m source depth. The data collected every 15 s are independently inverted using genetic algorithms (GA). $\Delta f = 5$ Hz is used. Since the environment is stable and range-independent, each inversion result represents an independent realization of the same environment with only range changing. Therefore, the histograms of the combined inversion results represent the PDFs for source and geoacoustic parameters. Since the range kept increasing, the histogram of the difference Δr_s between the GPS range and the inverted range is shown.

Three sets of inversions are performed. The first set uses frequency-only coherence B_f with range limited to ± 250 m around the GPS range. The second also uses B_f but the range limits are lowered by $c/\Delta f$ so that the GA focuses on the first alias, effectively tracking the aliased peak. The last set uses a conventional Bartlett function B_a around the true range. All the other source, array, and sediment parameters have the same limits. The inverted range values as a function of time are given in Fig. 3. Note that the second set of inverted ranges are 300 m less than the other two and the true range values. Due to its poor source localization capability [Fig. 2(a)], the conventional Bartlett result in a noisy track. The purpose is to see how the geoacoustic parameters are affected when the aliased peak is selected by the algorithm.

The set of inversions that track the aliased lobe [$B_f(r_{-1})$] in Fig. 2 creates biased estimates for the source range and depth, and water depth. Even though the MAPEX2000 environment is best represented by a single semi-infinite bottom for the frequencies used, our simulations showed that sediment thickness would be affected similarly. The sediment sound speed estimate still is accurate as all three methods give the same maximum *a posteriori* (MAP) estimate but the uncertainty in the c_{sed} estimate is increased. Both sediment density and attenuation are not well resolved with multi-peaked PDFs. Hence, even though the effects of range aliasing on the PDF are limited, it makes enough of a difference to give wrong MAP estimates while both regular B_f and B_a give similar MAP estimates.

4. Selection of the frequency sampling interval

Since the repetitive aliased lobes at every $c/\Delta f$ have consequences on both geoacoustic inversion and source localization, aliasing should be avoided if possible. A properly designed geoacoustic inversion should only search for the main lobe. The necessary frequency sampling for a desired geoacoustic search interval $r_0 \pm \Delta r$ should be determined as below.

(1) Ideally, it is desirable to avoid all aliased lobes from entering the search space $r_0 \pm \Delta r$. Since the width of the aliased lobe at the further range W_{r_1} is larger than W_{r-1} , the range where the aliased lobe centered at r_1 first appears is the closest point to the main lobe and the difference between that range and r_0 determines Δr . This will provide us with the limiting factor for how sparsely it is possible to sample in frequency while entirely avoiding the aliased lobes in the search space. This means computing r_{\min_i} for $i = 1$, which can be obtained using Eq. (4) and equating it to the upper limit of the search interval $r_0 + \Delta r$:

$$r_0 + \Delta r \leq \frac{c_{\min}}{c_{\max}} \left(r_0 + \frac{c}{\Delta f} \right), \quad (6)$$

$$\Delta f \leq \frac{c_{\min} c}{(r_0 + \Delta r) c_{\max} - r_0 c_{\min}}. \quad (7)$$

(2) However, often there is insufficient prior information about the environment to adequately predict c_{\min} and c_{\max} . This means it is not possible to know how wide the lobes are. Then one should at worst set the location of the next aliased lobe as the maximum Δr . This will avoid further aliased lobes and the center peak of the closest aliased lobes. The downside is that the side lobe structures of the closest aliased lobes will fall within the geoacoustic search interval. This results in a less strict formula for frequency sampling interval:

$$\Delta f \leq \frac{c}{\Delta r}. \quad (8)$$

For example, for a tracking application where the previous geoacoustic parameters and source location^{12,13} already are calculated and there is a good prior information about the current values, a smaller search interval width $2\Delta r$ is needed. So it is possible to use a large Δf and purposefully undersample the frequency response to reduce the computational cost without sacrificing performance. For the waveguide given in Fig. 1, using $\Delta r \geq 50$ m requires $\Delta f < 10$ Hz if Eq. (7) is used but $\Delta f < 30$ Hz using the less strict criteria.

5. Conclusions

Frequency undersampling can result in range aliasing and source localization errors and this will degrade geoacoustic inversion and source localization results. Range aliasing was demonstrated on data collected during the MAPEX2000 experiment.

Acknowledgments

This work was supported by the Office of Naval Research, under Grant Nos. N00014-05-1-0264 and N00014-09-1-0313.

References and links

- ¹Z.-H. Michalopoulou and M. B. Porter, "Matched-field processing for broad-band source localization," *IEEE J. Ocean. Eng.* **21**, 384–392 (1996).
- ²G. J. Orris, M. Nicholas, and J. S. Perkins, "The matched-phase coherent multi-frequency matched-field processor," *J. Acoust. Soc. Am.* **107**, 2563–2575 (2000).
- ³C. Soares and S. M. Jesus, "Broadband matched-field processing: Coherent and incoherent approaches," *J. Acoust. Soc. Am.* **113**, 2587–2598 (2003).

- ⁴A. B. Baggeroer, W. A. Kuperman, and H. Schmidt, "Matched field processing: Source localization in correlated noise as an optimum parameter estimation problem," *J. Acoust. Soc. Am.* **83**, 571–587 (1988).
- ⁵L. T. Fialkowski, T. C. Yang, K. Yoo, E. Kim, and D. K. Dacol, "Consistency and reliability of geoacoustic inversions with a horizontal line array," *J. Acoust. Soc. Am.* **120**, 231–246 (2006).
- ⁶J. Hermand, "Broad-band geoacoustic inversion in shallow water from waveguide impulse response measurements on a single hydrophone: Theory and experimental results," *IEEE J. Ocean. Eng.* **24**, 41–66 (1999).
- ⁷S. M. Jesus, M. B. Porter, Y. Stéphan, X. Démoulin, O. C. Rodríguez, and E. M. M. F. Coelho, "Single hydrophone source localization," *IEEE J. Ocean. Eng.* **25**, 337–346 (2000).
- ⁸E. K. Westwood, "Broadband matched-field source localization," *J. Acoust. Soc. Am.* **91**, 2777–2789 (1992).
- ⁹Z.-H. Michalopoulou, "Robust multi-tonal matched-field inversion: A coherent approach," *J. Acoust. Soc. Am.* **104**, 163–170 (1998).
- ¹⁰P. Gerstoft, W. S. Hodgkiss, W. A. Kuperman, H. Song, M. Siderius, and P. L. Nielsen, "Adaptive beamforming of a towed array during a turn," *IEEE J. Ocean. Eng.* **28**, 44–54 (2003).
- ¹¹M. R. Fallat, P. L. Nielsen, S. E. Dosso, and M. Siderius, "Geoacoustic characterization of a range-dependent ocean environment using towed array data," *IEEE J. Ocean. Eng.* **30**, 198–206 (2005).
- ¹²C. Yardim, P. Gerstoft, and W. S. Hodgkiss, "Geoacoustic and source tracking using particle filtering: Experimental results," *J. Acoust. Soc. Am.* **128**, 75–87 (2010).
- ¹³C. Yardim, Z.-H. Michalopoulou, and P. Gerstoft, "An overview of sequential Bayesian filtering in ocean acoustics," *IEEE J. Ocean. Eng.* **36**, 73–91 (2011).